Supplementary Material for: Variable exhumation rates and variable displacement rates: documenting a 10 Ma slowing of Himalayan shortening in western Bhutan

Methods-- USGS Central Mineral and Environmental Resources Science Center $^{40}Ar/^{39}Ar$ laboratory

The $^{40}Ar/^{39}Ar$ analyses were performed at the USGS in Denver, CO. High purity mineral grains of sample and standard were irradiated in separate irradiations of 3 and 20 megawatt hours, respectively, in the central thimble position of the USGS TRIGA reactor using cadmium lining to prevent nucleogenic production of ^{40}Ar. The neutron flux was monitored using Fish Canyon Tuff sanidine, with an age of 28.20 Ma ± 0.08 Ma (Kuiper et al., 2008) and isotopic production ratios were determined from irradiated CaF_2 and KCl salts. For these irradiations, the following production values were measured: Sample BU11-02, $(^{40}Ar/^{39}Ar)_K = 0$; $(^{36}Ar/^{37}Ar)_{Ca} = 2.533 \pm 0.0229 \times 10^{-4}$; and $(^{39}Ar/^{37}Ar)_{Ca} = 6.341 \pm 0.0306 \times 10^{-4}$; Sample BU11-04, $(^{40}Ar/^{39}Ar)_K = 0$; $(^{36}Ar/^{37}Ar)_{Ca} = 2.78 \pm 0.046 \times 10^{-4}$; and $(^{39}Ar/^{37}Ar)_{Ca} = 6.537 \pm 0.0337 \times 10^{-4}$. The irradiated samples and standards were loaded into 3 mm wells within a stainless steel planchette attached to a fully automated ultra high vacuum extraction line also constructed of stainless steel. Samples were incrementally heated until fusion using a 20W CO_2 laser equipped with a beam homogenizing lens. The gas was expanded and purified by exposure to a cold finger maintained at −135ºC and two hot SAES* GP50 getters. Following purification the gas was expanded into a Mass Analyser Products* 215-50 mass spectrometer and argon isotopes were measured by peak jumping using an electron multiplier operated in analog mode. Data were acquired during 10 cycles and time zero intercepts were determined by best-fit regressions to the data. Ages were calculated from data corrected for mass discrimination, blanks, radioactive decay subsequent to irradiation, and interfering nucleogenic reactions.

References cited:

Kuiper, K.F., Deino, A., Hilgen, F.J., Krijgsman, W., Renne, P.R. and Wijbrans, J.R., 2008. Synchronizing Rock Clocks of Earth History. Science 320, 500-504. doi: 10.1126/science.1154339.

Table SM1: White mica $^{40}Ar/^{39}Ar$ data

Figure SM1: $^{40}Ar/^{39}Ar$ age spectra and inverse isochron plots

Methods-- Arizona Radiogenic Helium Dating Laboratory (U-Th)/He dating

Zircon (U-Th)/He analyses followed the general procedures outlined in Reiners et al. (2004) and Reiners (2005). Individual zircon grains were selected from separates on the basis of size, morphology, and lack of inclusions. Grains lacking obvious fractures and with a minimum radius of 60 μm, with minimal to no inclusions, were selected. The dimensions of individual grains were measured from digital photomicrographs, using the approach outlined in Hourigan et al. (2005) for alpha-ejection corrections. Single grains were then packed into 1-mm Nb foil envelopes. Multiple foil packets were then placed in individual holes in a 30-hole planchette inside a ~7-cm laser cell pumped to $<10^{-9}$ torr. Individual packets were then heated for 15 minutes by a focused beam of a 1-2 W laser, to extract ^{4}He. The packets were then re-heated for 15 minutes, often multiple times, until ^{4}He yields were less than 1% of total. Standards of Fish Canyon Tuff (FCT) zircon (28.48±0.06 Ma [2σ], Schmitz and Bowring [2001]) were analyzed between every 5 unknowns.

Gas released from heated samples was spiked with 0.1-0.2 pmol ^{3}He, and condensed onto activated charcoal at the cold head of a cryogenic trap at 16 K. Helium was then released from the cold head at 37 K into a small volume (~50 cc) with an activated Zr-Ti alloy getter and the source of a Balzers quadrupole mass spectrometer (QMS) with a Channeltron electron multiplier. Peak-centered masses at approximately m/z of 1, 3, 4, and 5.2 were measured. Mass 5.2 establishes background, and mass 1 is used to correct mass 3 for HD and H3+. Corrected ratios of masses 4 to 3 were regressed through ten measurement cycles over ~15 s to derive an intercept value, which has an uncertainty of 0.05-0.5% over a $^{4}He/^{3}He$ range of $\sim10^{3}$, and compared with

the mean corrected ratio to check for significant anomalous changes in the ratio during analysis. Helium contents of unknown samples were calculated by first subtracting the average mass-1-corrected $^{4}He/^{3}He$ measured on multiple procedural blanks analyzed by the same method, from the mass-1-corrected $^{4}He/^{3}He$ measured on the unknown. This was then ratioed to the mass-1-corrected $^{4}He/^{3}He$ measured on a shot of an online reference ^{4}He standard analyzed with the same procedure. The resulting ratio of measured $^{4}He/^{3}He$ values was then multiplied by the moles of ^{4}He delivered in the reference shot.

After He extraction and measurement, foil packets were retrieved, transferred to Teflon vials, and spiked with 0.5-1.0 ng of ^{233}U and ^{229}Th. High-pressure digestion vessels were used for dissolution of the zircon and Nb foil packet. Natural-to-spike isotope ratios of U and Th were then measured on a high-resolution (single-collector) Element2 ICP-MS with all-PFA Teflon sample introduction equipment and sample preparation/analytical equipment. Blanks for zircon analyses were 2.6±0.5 pg U and 5.5±1.0 pg Th. Precision on measured U-Th ratios is typically better than 0.5% for zircon analyses. Propagated analytical uncertainties for typical zircon samples led to an estimated analytical uncertainty on (U-Th)/He ages of approximately 1-3% (1σ). In some cases, reproducibility of multiple aliquots approaches analytical uncertainty. However, in general, reproducibility of repeat analyses of (U-Th)/He ages is significantly worse than analytical precision. Thus (U-Th)/He ages typically show a much greater scatter and higher MSWD than expected based on analytical precision alone, and multiple replicate analyses of (U-Th)/He ages on several aliquots is necessary for confidence in a particular sample age.

For further information on the methods of (U-Th)/He dating at the Arizona Radiogenic Helium Dating Laboratory, refer to Reiners (2005), or to the laboratory's website: http://www.geo.arizona.edu/~reiners/arhdl/arhdl.htm. Single-grain ZHe ages and supporting data are shown on Table DR1, and weighted mean ZHe ages for each sample are shown on Table 1 in the text.

Table SM2: Single-grain zircon (U-Th)/He ages and supporting data

References cited:

Hourigan, J.K., Reiners, P.W., and Brandon, M.T., 2005, U-Th zonation-dependent alpha-ejection in (U-Th)/He chronometry. Geochim. Cosmochim. Acta 69, 3349-3365.

Ludwig, K.J., 2003, Isoplot 3.00: Berkeley Geochronology Center Special Publication 4, 70 p.

Reiners, P.W., Spell, T.L., Nicolescu, S., and Zanetti, K.A., 2004, Zircon (U-Th)/He thermochronometry: He diffusion and comparisons with $^{40}Ar/^{39}Ar$ dating: Geochim. Cosmochim. Acta 68, 1857-1887.

Reiners, P.W., 2005, Zircon (U-Th)/He thermochronometry: in: Reiners P. W., Ehlers, T. A. (Eds.), Low-Temperature Thermochronology: Techniques, Interpretations, and Applications. Rev. Mineral. Geochem. 58, 151-179. doi:10.2138/rmg.2005.58.6.

Schmitz, M.D., and Bowring, S.A., 2001, U-Pb zircon and titanite systematics of the Fish Canyon Tuff: an assessment of high-precision U-Pb geochronology and its application to young volcanic rocks: Geochimica et Cosmochimica Acta, v. 65, p. 2571-2587, doi:10.1016/S0016-7037(01)00616-0.

Discussion SM3: Methods of 1-D exhumation rate modeling

We used the AGE2EDOT program (Brandon et al., 1998) to quantify the permissible range of exhumation rates required to obtain the observed cooling ages. Our rationale for this 1-D thermal modeling approach follows the detailed justification presented in Thiede et al. (2009), which is based on 1) the results of Whipp et al. (2007), who found that cooling ages are the most sensitive to the vertical (i.e., 1-D exhumation) component of the kinematic field in rapidly-eroding orogens, and 2) thermal modeling studies (Ehlers et al., 2005; Reiners and Brandon, 2006) that suggest that thermal transients have minimal effects on the rapid exhumation rates typical to the Himalaya.

The modeling was used to identify the permissible range of exhumation rates required to obtain the MAr, ZHe, and AFT cooling ages. This was performed by inputting estimates for thermo-physical properties of Himalayan rocks for individual models for each thermochronometer. Input model parameters included: 1) Thermal diffusivity (κ), which was

varied between 21, 38, and 48 km^2/myr, which correspond to thermal conductivity values of 1.531, 2.770, and 3.498 W/mK, respectively. These represent the low, center, and high values of the 1.5-3.5 W/mK range of thermal conductivity estimated for Himalayan rocks (Ray et al., 2007; Herman et al., 2010), and the center of the 2.5-3.0 W/mK thermal conductivity range estimated by Whipp et al. (2007). 2) Uniform internal heat production rate (H_T), which was varied between 11, 26, and 33°C/myr, which corresponds to volumetric heat production values of 0.802, 1.895, and 2.405 $\mu W/m^3$, respectively. These represent the low, center and high values of the 0.8-2.4 $\mu W/m^3$ volumetric heat production estimated for LH rocks (Herman et al., 2010). 3) For layer depth to constant temperature (L), a value of 30 km was used, based on petrologic estimates for the peak depth of GH rocks in Bhutan (Daniel et al., 2003; Corrie et al., 2012). 4) For surface temperature (T_S), 20°C, the average surface temperature of western Bhutan (http://www.nepaltravels.com/bhutan/general_information/weather_climate.htm) was used. 5) Three surface thermal gradients (G_T) were modeled: 20, 30, and 40°C/km. This parameter was the largest unknown, because data directly constraining the geothermal gradient in Bhutan are not available. Petrologic estimates of peak temperatures and pressures obtained from GH rocks in eastern and central Bhutan indicate that geothermal gradients may have been as low as ca. 20-25°C/km at ca. 22 Ma (Daniel et al., 2003; Corrie et al., 2012). However, since nearly all of our cooling ages come from LH rocks, and are much younger (ca. 16-3 Ma total range), we cautiously chose to model a large range of geothermal gradients (20-40°C/km) in the absence of more direct constraints. The effects of these different geothermal gradients had the most significant effect on the permissible range of exhumation rates, and far outweighed the effects of varying thermal diffusivity (thermal conductivity) and internal heat production (volumetric heat production).

Temperature-time (T-t) graphs were constructed for seven different regions where data were available to determine cooling from peak temperatures to modern temperatures. The data used in their construction are shown in Table DR3. For each T-t path, we used AGE2EDOT modeling results to estimate the range of closure temperatures, depth to closure, and the permissible exhumation rates based on the age and error associated with a given sample. Temperature errors were obtained from the upper and lower limits of the peak temperature range for each sample and from the closure temperature range for each thermochronometer estimated by AGE2EDOT modeling. These were incorporated along with uncertainty in ages to make the

gray swath, which shows the permissible variation in the T-t path. For each segment of the T-t path between successive data points, we calculated the rate between each chronometer using the method outlined by Thiede et al. (2009). The exhumation rate (E_2) between the AFT system (E_0t_0) and the ZHe system (E_1t_1) is $E_2 = [(E_0t_0) - (E_1t_1)]/ (t_1-t_0)$, while the exhumation rate between the MAr and the ZHe system must include the intermediate rates from the previous systems $E_3 = [(E_0t_0) - (E_2t_2)- (E_1t_1)]/ (t_2-(t_1-t_0))$. The exhumation rate (mm/yr) for a 30°C/km geothermal gradient and the center age is shown in black text. The gray text indicates the permissible range in exhumation rates for a 40°C/km geothermal gradient and the high age error bar (low exhumation rates) and a 20°C/km geothermal gradient and the low age error bar (high exhumation rates). Due to the difference in error magnitude between thermochronologic systems (i.e., AFT analyses and ZHe analyses), the "low exhumation rate between analyses" may have a higher rate than the calculated "high exhumation rate" or "center exhumation rate". This is because the difference between the ages (t_0-t_1), used to calculate the transient exhumation rate becomes a much smaller number when the error bars on t_0 are significantly larger than the error bars for age on t_1. Regardless of these discrepancies, we always report the highest and lowest exhumation rates on Figure 2.

Region 6: Northern Paro window

Prograde (burial) monazite growth in GH rocks until 20.8 ± 1.1 Ma indicates the youngest possible time for achievement of peak temperatures. Peak temperatures in western Bhutan are identified only through mineral assemblages (Tobgay et al., 2012). The presence of partially-melted, kyanite-bearing paragneiss with sillimanite and K- feldspar requires that these rocks attained a temperature greater than 700°C at a pressure of 8 kbar (e.g., Daniel et al., 2003; Spear et al., 1999). However, garnet-biotite thermometry on rocks of similar composition in eastern Bhutan and Nepal show peak temperatures between 750-800°C (Daniel et al., 2003; Kohn 2008). The peak temperature of similar assemblages and the delay time from achievement of peak temperatures to cooling below 700°C (5-10 Myr) suggests that peak temperatures in GH rocks in western Bhutan were as high as 750-800°C. A decrease in temperature, initiating at 15.1 ± 0.4 Ma, is indicated by the age of the oldest retrograde monazite (n=18) from the base of the GH section. Retrograde monazite continued to grow from 10.5-13.3 Ma, indicating cooling of rocks below 700°C (the approximate minimum temperature for muscovite dehydration-melting [Spear et al., 1999; Pyle and Spear, 2003; Kohn et al., 2005]), through this time window.

Muscovite cooled below 325-400°C at 11.4 Ma ± 1.5 Ma. The similar ages for both retrograde monazite growth and muscovite closure, particularly taking into account the range in cooling ages, requires incredibly fast exhumation from 700 to 400-325°C. Corresponding exhumation rates range from 7.6–50 mm/yr for a 30°C/km geothermal gradient with a total exhumation rate range of 5.7–75 mm/yr for 40°C/km and 20°C/km geothermal gradients, respectively. ZHe ages from the northern Paro window have a combined age of 6.5 ± 0.5 Ma and are modeled to have cooled from ~400°C to 190°C at rates of 0.8–1.5 mm/yr for a 30°C/km geothermal gradient, and a total exhumation rate range of 0.6–2.2 mm/yr. AFT data display a wider range of ages in the northern Paro window region, between 2.6 and 6.1 Ma (Fig. 1). A weighted mean of these ages suggests a combined age of 4.7 ± 0.6 Ma. Our modeling indicates that this region continued to cool from 190°C to 121-124°C at rates of 1.0–1.7 mm/yr (30°C/km geothermal gradient) with a total range of 0.8–2.6 mm/yr. Exhumation rates to the present continued to slow to 0.6-0.8 mm/yr, with a total range of 0.5-1.3 mm/yr. The total exhumation path for the northern window highlights rapid exhumation initiating at ~12 Ma and systematically decreasing towards the present.

Region 5: Southern Paro window

Peak temperatures and ages in the southern portion of the Paro window are similar to those in the north; however, rocks in this region cooled below 700° C at 14.3 ± 0.7 Ma (Fig. 1B). A bedrock MAr age of 11.6 ± 0.1 Ma requires the rocks to have cooled from 700 to 400-324°C at modeled rates of 4.1-5.2 mm/yr with a permissible range of rates from 3.0-7.9 mm/yr. A ZHe age of 7.6 ± 0.1 Ma indicates that these rocks continued to cool at rates of 1.1-1.7 mm/yr (0.8-2.5 mm/yr; parentheses mark total range in cooling rates). An AFT age of 3.5± 0.6 Ma indicates that exhumation rates progressively slowed to 0.5-0.6 mm/yr, with a permissible range between 0.4-0.9. The young AFT age also suggests that exhumation rates from 3-4 Ma to present may be slightly higher at 0.8-1.2 mm/yr (0.6-1.8 mm/yr). Exhumation rates in the southern Paro window highlight that the period of fastest exhumation is from ~14.3-7.6 Ma.

Region 4: Chukha

The southernmost exposure of the Paro Formation is located at a narrow window through the MCT near Chukha (Fig. 1). Here, peak temperatures were reached at 20.8 Ma, and rocks

cooled below 700°C at 12.9 ± 1.5 Ma (Fig. 1). A MAr cooling age of 11.4 ± 0.1 Ma indicates that the most rapid period of cooling occurred at rates of 4.4-62.5 mm/yr (3.3-93.7 mm/yr). Similar to samples from the northern Paro window, the calculation of very fast exhumation rates is due to the similarity in age of retrograde monazite growth and cooling through the MAr closure temperature, particularly taking into account the range of measured monazite ages. Slower cooling rates of 1.5-2.3 mm/yr (1.1-3.4 mm/yr) occurred from 11.4 Ma to 8.4 Ma, and continue to slow from 8.4 Ma (ZHe) to 6.5 Ma (AFT) with rates of 0.9-2.0 mm/yr (0.7-3.0). The slowest exhumation rates are from 6.5 Ma to present, at 0.5-0.6 mm/yr (0.3-0.9 mm/yr).

Region 3: Lower Lesser Himalayan rocks immediately under MCT

Lower LH rocks exposed immediately beneath the MCT experienced peak temperatures of 500°C and are associated with prograde monazite growth at 15 ± 2.4 Ma (Tobgay at al., 2012). From peak temperatures these rocks cooled quickly to 187-189°C by 9.2 ± 0.2 Ma at rates of 1.3-2.8 mm/yr (1.0-4.3 mm/yr) (Fig. 2). Between 9 Ma and 1.4 Ma, cooling slowed dramatically to 0.2-0.3 mm/yr (0.2-0.4 mm/yr). Since 1.4 Ma, exhumation rates have increased with rocks cooling from 130°C to 20°C at rates of 1.8-3.8 mm/yr (1.4-7.3 mm/yr).

Region 2: Upper LH duplex (northern Baxa Group)

Upper LH rocks in the northern exposed portions of the Baxa Group duplex experienced peak temperatures of 300-350°C between 9 and ~12 Ma, the window of time that lower LH sample BU08-135 experienced rapid exhumation. Exhumation of northern Baxa Group rocks from 300-350° to 190-193°C occurred between 9 and 6.2 Ma at rates of 0.7-1.8 mm/yr (0.5-2.7 mm/yr). From 6.2 Ma (ZHe) to 1.8 Ma (AFT) exhumation slowed to 0.4-0.5 mm/yr (0.3-0.7 mm/yr). Similar to the lower LH samples, 1.8 Ma to the present marked an increase in exhumation from 133° to 20°C at rates of 1.5-3.2 mm/yr (1.2-4.8 mm/yr).

Region 1: Upper LH duplex (southern Baxa Group)

Although most samples from the Baxa Group have ZHe cooling ages of ~9 Ma, three samples from the southern part of the Baxa Group duplex all record young 3.4-1.9 Ma ZHe cooling ages. Modeling suggests that these rocks cooled from 198-203°C to 20°C at rates of 1.7-3.5 mm/yr (1.3-5.2 mm/yr).

Table SM3: Data table showing results from exhumation rate modeling. Cells R-T, Y-AA, and AF-AH indicate exhumation rates between each temperature-time data point for a given sample, for all three geothermal gradients using the high-rate, low rate and center rate, respectively. These rates were used to calculate the T-t paths in Figure 2 in the text. Because there is age overlap (given the large uncertainty on monazite ages) between monazite and MAr ages, we used an age immediately older than the low MAr estimate for the low error monazite estimate (for example the low error monazite age is stated as 11.2 Ma in cells E8 and N8, even though analytically, the age is as low as 10.44 Ma. This is under the assumption that the retrograde monazite is always older and crystallized at higher temperatures than the MAr system.

References cited:

Brandon, M. T., Roden-Tice, M. K., and Garver, J.I., 1998. Late Cenozoic exhumation of the Cascadia accretionary wedge in the Olympic Mountains, northwest Washington State. Geological Society of America Bulletin 110, 985–1009, doi:10.1130/0016-7606(1998)110<0985:LCEOTC>2.3.CO;2.

Corrie, S.L., Kohn, M.J., McQuarrie, N., and Long, S.P., 2012. Flattening the Bhutan Himalaya. Earth Planet. Sci. Lett. 349-350, 67-74, doi:10.1016/j.epsl.2012.07.001.

Daniel, C. G., Hollister, L. S., Parrish, R.R., and Grujic, D., 2003. Exhumation of the Main Central Thrust from lower crustal depths, eastern Bhutan Himalaya. J. Metamorph. Geol. 21, 317–334, doi:10.1046/j.1525-1314.2003.00445.x.

Ehlers, T. A., Chaudhri, T., Kumar, S., Fuller, C.W., Willett, S.D., Ketcham, R.A., Brandon, M.T., Belton, D.X., Kohn, D.B., Gleadow, A.J.W., Dunai, T.J., and Fu, F.Q., 2005. Computational tools for low-temperature thermochronometer interpretation: in: Reiners P. W., Ehlers, T. A. (Eds.), Low-Temperature Thermochronology: Techniques, Interpretations, and Applications. Rev. Mineral. Geochem. 58, 589–622. doi:10.2138/rmg.2005.58.22.

Herman, F., Copeland, P., Avouac, J.-P., Bollinger, L., Maheo, G., LeFort, P., Rai, S., Foster, D., Pecher, A., Stuwe, K., and Henry, P., 2010. Exhumation, crustal deformation, and thermal structure of the Nepal Himalaya derived from the inversion of thermochronological and thermobarometric data and modeling of the topography. J. Geophys. Res. 115, B0647, doi:10.1029/2008JB006126.

Kohn, M.J., Wieland, M.S., Parkinson, C.D., Upreti, B.N., 2005. Five generations of monazite in Langtang gneisses: implications for chronology of the Himalayan metamorphic core. J. Metamorph. Geol. 23, 399–406.

Pyle, J.M., Spear, F.S., 2003. Four generations of accessory-phase growth in low-pressure migmatites from SW New Hampshire. Am. Mineral. 88, 338–351.

Ray, L., Bhattacharya, A., and Roy, S., 2007. Thermal conductivity of Higher Himalayan Crystallines from Garhwal Himalaya, India. Tectonophysics 434, 71–79. doi:10.1016/j.tecto.2007.02.003.

Reiners, P. W., and Brandon, M.T., 2006. Using thermochronology to understand orogenic erosion: Ann. Rev.Earth Planet. Sci. 34, 419–466. doi: 10.1146/annurev.earth.34.031405.125202.

Spear, F.S., Kohn, M.J., Cheney, J.T., 1999. P–T paths from anatectic pelites. Contrib. Mineral. Petrol. 134, 17–32.

Thiede, R.C., Ehlers, T.A., Bookhagen, B., and Strecker, M.R., 2009. Erosional variability along the northwest Himalaya. Tectonics. 114, F01015, doi:10.1029/2008JF001010.

Tobgay T, McQuarrie, N., Long, S.P., Kohn, M.J., Corrie, S.L., 2012. The age and rate of displacement along the Main Central Thrust in the western Bhutan Himalaya. Earth Planet. Sci. Lett. 319-320, 146-158, doi:10.1016/j.epsl.2011.12.005.

Whipp, D. M., Ehlers, T.A., Blythe, A.E., Huntington, K.W., Hodges, K.V., and Burbank, D.W., 2007. Plio-Quaternary exhumation history of the central Nepalese Himalaya: 2. Thermokinematic and thermochronometer age prediction model.Tectonics. 26, TC3003, doi:10.1029/2006TC001991.

Watts	Relative Isotopic Abundances										Derived Results				
	^{40}Ar		^{39}Ar		^{38}Ar		^{37}Ar		^{36}Ar		^{39}Ar Mol	^{39}Ar %	% $^{40}Ar^{*}$	Age (Ma)	
	±1S		±1S		±1S		±1S		±1S		$\square 10^{-14}$	of total		±1S	
BU-11-02; single muscovite grain, J = 0.000669 +/- 0.000002															
0.2	4.6555	0.0162	0.4378	0.0022	0.0056	0.0006	0.0312	0.0042	0.0021	0.0006	0.01	0.9	86.6	11.1	0.5
0.2	8.4834	0.0192	0.8032	0.0031	0.0083	0.0006	0.0522	0.0043	0.0012	0.0006	0.02	1.6	96.0	12.2	0.3
0.3	9.6389	0.0221	0.9123	0.0037	0.0106	0.0006	0.0660	0.0046	0.0026	0.0006	0.02	1.8	92.0	11.7	0.2
0.3	11.2129	0.0296	0.9516	0.0033	0.0147	0.0007	0.1059	0.0044	0.0051	0.0006	0.02	1.9	86.7	12.3	0.2
0.4	40.7104	0.0453	3.8854	0.0073	0.0520	0.0010	0.4130	0.0052	0.0116	0.0006	0.09	7.7	91.7	11.6	0.1
0.4	49.7153	0.0881	4.9611	0.0096	0.0648	0.0008	0.4067	0.0053	0.0098	0.0006	0.11	9.9	94.2	11.4	0.1
0.5	57.8270	0.0931	5.9960	0.0093	0.0768	0.0009	0.4701	0.0054	0.0044	0.0006	0.13	11.9	97.8	11.4	0.0
1.5	234.8446	0.2105	######	0.0400	0.3071	0.0016	1.1403	0.0065	0.0194	0.0007	0.54	48.2	97.6	11.4	0.0
1.8	16.6304	0.0194	1.7028	0.0042	0.0222	0.0007	0.0053	0.0044	0.0011	0.0006	0.04	3.4	98.1	11.5	0.1
2.0	15.8884	0.0223	1.6680	0.0130	0.0207	0.0008	0.0058	0.0041	0.0002	0.0006	0.04	3.3	99.6	11.4	0.2
2.5	30.4280	0.0416	3.1131	0.0089	0.0397	0.0008	0.0042	0.0041	0.0001	0.0006	0.07	6.2	99.9	11.8	0.1
3.0	16.3136	0.0202	1.6629	0.0064	0.0204	0.0007	0.0000	0.0043	0.0000	0.0006	0.04	3.3	100.0	11.8	0.1
BU-11-04; single muscovite grain, J = 0.004159 +/- 0.000003															
0.3	3.4008	0.0320	1.8420	0.0053	0.0248	0.0005	0.0047	0.0020	0.0003	0.0005	0.04	1.0	97.4	13.4	0.6
0.4	13.3392	0.0397	7.6971	0.0094	0.1056	0.0011	0.0118	0.0025	0.0028	0.0003	0.17	4.1	93.8	12.1	0.1
0.6	16.4680	0.0404	9.7148	0.0130	0.1295	0.0011	0.0025	0.0024	0.0039	0.0003	0.21	5.2	93.1	11.8	0.1
0.7	27.4324	0.0549	######	0.0140	0.2169	0.0013	0.0038	0.0017	0.0063	0.0004	0.36	8.6	93.2	11.8	0.1
0.9	29.2291	0.0680	######	0.0180	0.2296	0.0015	0.0020	0.0018	0.0055	0.0004	0.39	9.4	94.4	11.7	0.1
1.0	37.0571	0.0461	######	0.0300	0.2971	0.0014	0.0069	0.0018	0.0051	0.0004	0.50	12.0	95.9	11.7	0.0
1.2	54.2519	0.0725	######	0.0440	0.4443	0.0019	0.0027	0.0028	0.0067	0.0004	0.76	18.2	96.3	11.4	0.0
1.3	57.1736	0.0500	######	0.0460	0.4637	0.0017	0.0097	0.0017	0.0081	0.0004	0.78	18.7	95.8	11.6	0.0
1.5	59.5921	0.0500	######	0.0520	0.4902	0.0020	0.0057	0.0018	0.0042	0.0004	0.82	19.8	97.9	11.7	0.0
1.6	5.6746	0.0323	3.8250	0.0058	0.0502	0.0006	0.0000	0.0023	0.0002	0.0003	0.08	2.0	98.8	11.0	0.2
1.8	3.2296	0.0366	2.0909	0.0054	0.0280	0.0005	0.0052	0.0018	0.0003	0.0003	0.05	1.1	97.6	11.3	0.3

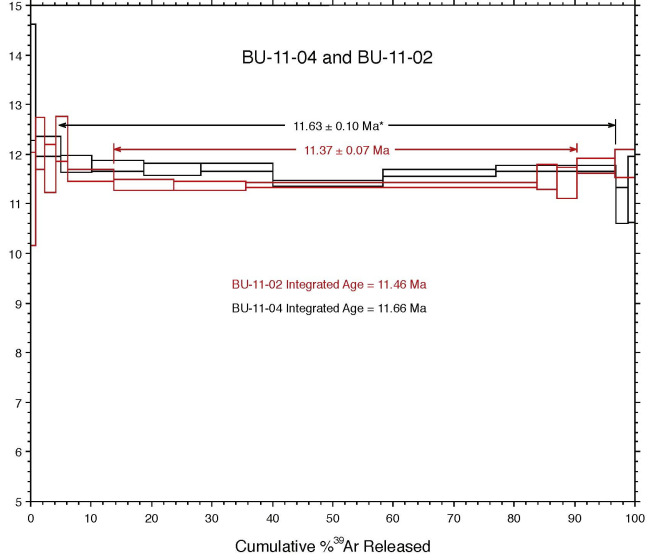

BU-11-04

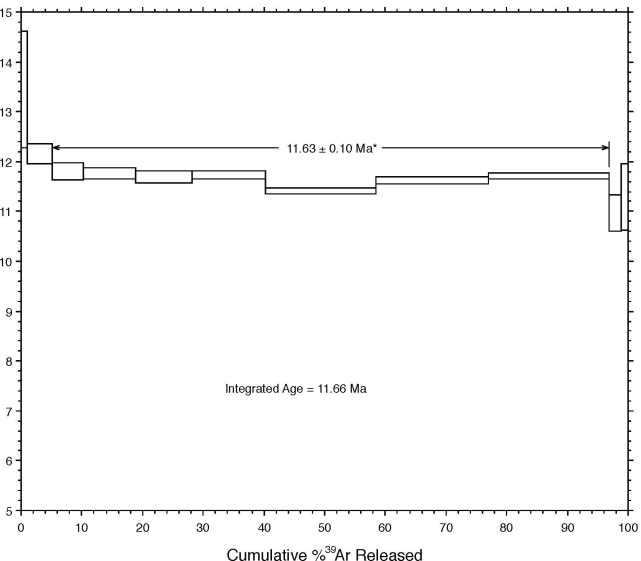

BU-11-02

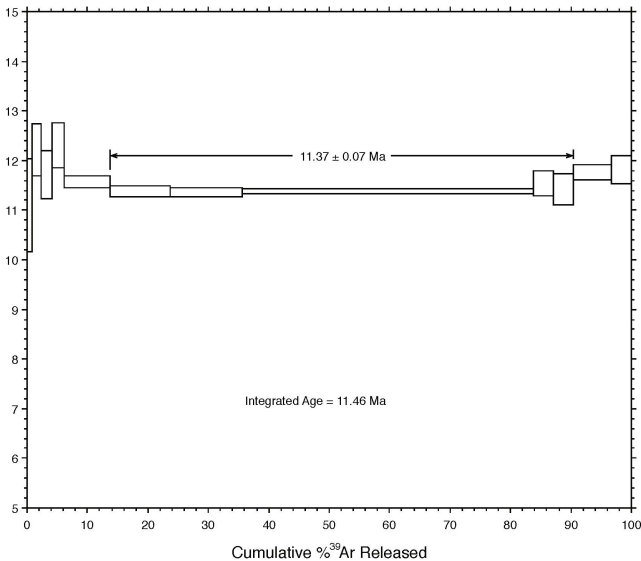

Table DR1: Single grain zircon (U-Th)/He ages and supporting data

Sample name	ng U	ng Th	Raw age (Ma)	Est 1σ error	Mass (µg)	half-width (µm)	U (ppm)	Th (ppm)	Th/U
BU07-60_z1	0.32	0.19	2.25	0.03		36.34	215	126	0.60
BU07-63_z1	1.21	1.05	4.36	0.06		25.69	1193	1031	0.89
BU07-63_z2	2.20	0.30	5.44	0.08		51.62	522	72	0.14
weighted mean									
BU07-73_z1	0.77	0.75	11.54	0.15		41.46	332	323	1.00
BU07-73_z2	1.25	1.15	9.66	0.13		46.60	384	352	0.94
BU07-73_z3	6.78	0.52	9.18	0.25		63.95	813	62	0.08
weighted mean									
BU07-75_z1	0.43	0.20	5.69	0.08		39.18	195	93	0.49
BU07-75_z2	0.45	0.62	5.82	0.07		41.73	182	251	1.42
BU07-75_z3	0.83	0.25	5.55	0.08		43.80	259	78	0.31
weighted mean									
BU07-76_z2	2.93	0.83	2.28	0.04		47.72	800	226	0.29
BU07-79_z2	0.78	0.35	4.63	0.07		55.95	121	53	0.45
BU07-79_z3	2.26	2.80	5.76	0.08		61.93	265	329	1.27
BU07-79_z5	1.06	0.67	5.02	0.07		50.98	211	133	0.65
weighted mean									
BU08-135_z1	11.97	1.39	7.14	0.36		73.43	873	102	0.12
BU08-135_z2	9.11	0.17	7.70	0.43		72.10	702	13	0.02
BU08-135_z3	4.77	0.72	7.56	0.13		61.18	614	93	0.16
weighted mean									
BU10-64_z1	2.41	0.93	2.21	0.04	5.50	64.34	438	169	0.40
BU10-64_z2	0.80	0.80	4.09	0.08	3.78	41.66	210	211	1.03
BU10-64_z3	3.12	0.60	2.54	0.06	4.89	53.71	639	123	0.20
weighted mean									
BU10-65_z1	0.52	0.50	1.19	0.05	0.93	31.78	555	540	1.00
BU10-65_z2	1.14	0.22	1.32	0.05	1.12	34.30	1023	193	0.19
weighted mean									
BU10-68_z1	0.23	0.47	4.01	0.12	0.89	31.57	263	527	2.05
BU10-68_z2	0.76	0.36	4.07	0.10	1.11	34.25	686	321	0.48
weighted mean									
BU10-71_z1	0.56	0.16	6.25	0.09		44.40	170	50	0.30

BU10-89_Z_2	1.96	1.04	8.45	0.19	8.14	58.86	241	128	0.54
BU10-89_Z_3	5.39	3.31	7.85	0.17	17.86	67.71	301	185	0.63
weighted mean									
BU10-90_Z_1	0.83	0.71	7.32	0.16	4.69	52.98	177	152	0.88
BU10-90_Z_2	0.93	0.28	4.92	0.13	0.99	30.91	943	286	0.31
BU10-90_Z_3	0.13	0.18	6.46	0.22	0.84	28.82	155	209	1.38
weighted mean									
BU10-93_Z_2	1.92	0.87	6.94	0.16	3.48	50.51	550	250	0.47
BU10-93_Z_3	2.01	1.00	6.17	0.14	3.93	52.96	511	254	0.51
weighted mean									
BU11-01_z1	1.31	0.58	8.30	0.15		51.27	283	126	0.45
BU11-01_z2	1.95	0.64	7.25	0.13		60.03	260	86	0.34
BU11-01_z3	6.50	2.32	6.72	0.10		77.94	440	157	0.37
weighted mean									
BU11-02_z1	0.98	0.50	6.34	0.09		43.76	356	184	0.53
BU11-02_z2	0.78	0.18	5.47	0.08		46.88	246	57	0.24
BU11-02_z3	1.58	1.10	6.46	0.08		50.05	428	300	0.72
weighted mean									
BH-411_z1	16.30	2.03	5.45	0.21		84.78	784	98	0.13
BH-411_z2	10.08	1.17	5.26	0.12		73.60	771	89	0.12
BH-411_z3	6.41	1.29	5.40	0.14		71.70	531	107	0.21
weighted mean									
BH-424_z1	3.64	2.65	7.22	0.15		59.63	441	320	0.74
BH-424_z2	2.07	0.31	4.46	0.07		54.37	371	56	0.15
BH-424_z3	1.60	0.92	5.04	0.12		50.93	406	233	0.59
weighted mean									
BH-432_z1	0.56	0.26	5.18	0.09		39.29	250	114	0.47
BH-432_z2	1.23	0.50	4.60	0.08		41.10	448	182	0.42
BH-432_z3	0.87	0.11	4.70	0.08		38.65	465	59	0.13
weighted mean									
BH-413_z1	0.34	0.30	4.99	0.08		49.99	81	71	0.91
BH-413_z2	1.20	1.70	5.67	0.06		51.61	250	353	1.45
BH-413_z3	0.86	0.65	5.26	0.07		57.83	130	99	0.78
weighted mean									
BH-415_z1	71.76	14.41	5.63	0.85		82.92	2730	548	0.21
BH-415_z2	56.59	10.78	4.74	0.32		92.64	2085	397	0.20
BH-415_z3	61.69	8.07	5.13	0.57		71.94	3617	473	0.13

weighted mean								
BH-401_z1	2.88	0.83	4.02	0.06	59.90	398	114	0.29
BH-401_z2	5.62	0.71	3.92	0.06	61.11	636	81	0.13
BH-401_z3	2.72	0.66	4.02	0.06	57.27	427	103	0.25
weighted mean								
BH-109_z1	19.43	1.48	5.49	0.29	84.18	906	69	0.08
BH-109_z2	3.60	0.71	4.62	0.08	59.19	502	99	0.20
BH-109_z3	15.75	2.61	6.20	0.40	89.35	634	105	0.17
weighted mean								
F-01a_z1	0.43	0.26	4.91	0.07	35.87	299	180	0.62
F-01a_z2	0.67	0.58	4.10	0.06	45.27	206	181	0.90
weighted mean								
F-04_z1	2.37	0.46	7.15	0.13	56.77	380	73	0.20
F-04_z2	2.18	0.26	6.19	0.10	48.01	624	75	0.12
F-04_z3	0.66	0.11	8.31	0.14	40.19	278	46	0.17
weighted mean								
F-07_z1	0.83	0.16	5.56	0.09	42.08	307	58	0.19
F-07_z2	0.45	0.16	5.20	0.09	37.56	209	73	0.36
weighted mean								
F-05_z1	1.70	0.37	5.84	0.08	42.48	655	141	0.22
F-05_z2	1.60	0.23	5.00	0.08	44.51	557	81	0.15
F-05_z3	2.84	0.29	6.16	0.10	48.44	845	88	0.11
weighted mean								

Notes:

1. [a]Ft is alpha ejection correction for zircon (Reiners, 2005).
2. weighted means calculated from Isoplot program (Ludwig, 2003). 1σ internal error is reported.
3. half-width is c-axis perpendicular half-width.

^{4}He (nmol/g)	^{a}Ft	Corrected age (Ma)	Est 1σ error
2.96	0.67	3.36	0.05
33.74	0.55	7.88	0.10
15.79	0.76	7.12	0.10
		7.64	0.16
25.37	0.71	16.36	0.21
24.26	0.74	13.13	0.17
40.83	0.81	11.37	0.31
		13.26	0.21
6.64	0.69	8.20	0.11
7.57	0.70	8.26	0.10
8.26	0.72	7.66	0.11
		8.05	0.13
10.45	0.75	3.06	0.05
3.32	0.78	5.94	0.09
10.63	0.80	7.25	0.10
6.55	0.76	6.62	0.09
		6.60	0.10
34.42	0.83	8.60	0.44
29.19	0.83	9.30	0.52
25.83	0.80	9.47	0.17
		9.09	0.15
5.68	0.02	2.72	0.05
5.73	0.01	5.46	0.10
9.13	0.02	3.18	0.07
		3.24	0.08
4.37	0.03	1.80	0.07
7.59	0.02	1.92	0.07
		1.86	0.10
8.40	0.02	6.17	0.19
16.71	0.02	5.96	0.14
		6.03	0.23
6.09	0.73	8.58	0.12

12.36	0.02	10.32	0.23
14.61	0.02	9.30	0.20
		9.74	0.30
8.41	0.02	9.26	0.20
26.78	0.02	7.39	0.19
7.13	0.02	10.11	0.34
		8.54	0.26
22.80	0.02	8.93	0.21
19.00	0.02	7.86	0.17
		8.93	0.26
14.01	0.76	10.92	0.19
10.94	0.79	9.13	0.16
17.28	0.84	8.01	0.12
		9.06	0.18
13.66	0.72	8.78	0.12
7.65	0.74	7.37	0.11
17.38	0.75	8.58	0.11
		8.35	0.13
23.65	0.85	6.40	0.25
22.40	0.83	6.33	0.15
16.14	0.83	6.54	0.17
		6.42	0.11
20.04	0.79	9.13	0.19
9.21	0.78	5.75	0.09
12.50	0.76	6.65	0.16
		6.80	0.11
7.71	0.69	7.46	0.12
12.14	0.71	6.51	0.12
12.10	0.69	6.78	0.11
		6.87	0.13
2.62	0.75	6.63	0.10
10.19	0.76	7.50	0.09
4.34	0.78	6.71	0.09
		6.99	0.11
86.50	0.85	6.63	1.00
55.54	0.86	5.49	0.37
102.69	0.83	6.20	0.69

		6.03	0.10
9.19	0.79	5.07	0.07
13.79	0.80	4.91	0.08
9.74	0.79	5.12	0.08
		5.03	0.08
27.19	0.85	6.45	0.34
13.03	0.79	5.83	0.10
21.96	0.86	7.21	0.46
		6.40	0.11
9.02	0.67	7.36	0.11
5.50	0.73	5.63	0.08
		6.22	0.13
15.27	0.78	9.13	0.16
21.33	0.75	8.27	0.14
12.90	0.70	11.82	0.20
		9.13	0.18
9.56	0.71	7.77	0.12
6.34	0.68	7.62	0.13
		7.70	0.18
21.61	0.72	8.15	0.12
15.48	0.73	6.85	0.11
28.66	0.75	8.21	0.13
		7.66	0.13

Northern Samples

BU08-24, BU08-01 (m), BH-432, BH-424, BH109, BH- 411, BH-415 (ZHe)

BH 109, F17, f09, f08 (aft)

Analysis	Age and error (Ma)	Center age (Ma)	Low error age (Ma)	High error age (Ma)	T closure range (°C)	
Peak T	20.8 ± 1.1	20.8	19.7	21.9		750
Monazite	12.04 ± 1.6	12.04	11.2	13.64		700
MAr	11.5 ± 0.5	11.5	11	12	324-400	
ZHe	6.46 ± 0.10	6.46	6.36	6.56	190-193	
AFT	4.67 ± 0.55	4.67	4.12	5.22	121-124	
modern	0	0	0	0		

Southern Paro Window

BU11-04, BU08-130, BU07-75

Peak T	20.8 ± 1.1	20.8	19.7	21.9		750
Monazite	14.3 ± 0.69	14.3	13.61	14.99		700
MAr	11.8 ± 0.1	11.8	11.7	11.9	324-400	
ZHe	7.64 ± 0.13	7.64	7.51	7.77	188-190	
AFT	3.5 ± 0.6	3.5	2.9	4.1	125-127	
modern	0	0	0	0		

Chukha

BU11-02, BU08-131, F06

Peak T	20.8 ± 1.1	20.8	19.7	21.9		750
Monazite	12.88 ± 1.45	12.88	11.43	14.33		700
MAr	11.37 ± 0.1	11.37	11.27	11.47	324-400	
ZHe	8.35 ± 0.13	8.35	8.22	8.48	188-190	
AFT	6.5 ± 0.8	6.5	5.7	7.3	118-121	
modern	0	0	0	0		

LH (directly under MCT)

F04 and BU08-135

Peak T/Monaz	15 ± 2.4	15	12.6	17.4		500
ZHe	9.18 ±0 .23	9.18	8.95	9.41	186-189	
AFT	1.4± 0.6	1.4	0.8	2	130-136	
modern	0	0	0	0		

upper LH duplex (north)

F01a

Peak T	9-12 Ma	10.5	9	12	300-350	
ZHe	6.22 ± 0.13	6.22	6.09	6.35	190-193	
AFT	1.8 ± 0.6	1.8	1.2	2.4	130-136	
modern	0	0	0	0		

upper LH duplex (south)

BU10-65	ZHe	1.86± 0.1	1.86	1.76	1.96	201-203
	modern	0	0	0	0	
upper LH duplex (south)						
BU07-60	ZHe	3.36 ± 0.05	3.36	3.31	3.41	198-202
	modern	0	0	0	0	

Center T (°C)	Low T (°C)	High T (°C)	Total exhumation rate range since cooling age (mm/yr)			Low error age (Ma)
			20°C/km	30°C/km	40°C/km	
750	750	750	1.71-1.90	1.14-1.27	0.86-0.95	19.7
700	700	700	2.57-3.13	1.71-2.08	1.28-1.56	11.2
397	324	400	1.38-1.82	0.92-1.21	0.69-0.91	11
192	190	193	1.45-1.52	0.97-1.01	0.72-0.76	6.36
122	121	124	1.16-1.49	0.77-1.0	0.58-0.75	4.12
20	20	20	0	0	0	0
750	750	750	1.71-1.90	1.14-1.27	0.86-0.95	19.7
700	700	700	2.33-2.57	1.56-1.71	1.17-1.29	13.61
397	324	400	1.36-1.71	0.91-1.14	0.68-0.85	11.7
190	188	191	1.12-1.27	0.81-0.85	0.6-0.64	7.51
125	123	127	1.5-2.19	1.0-1.46	0.75-1.09	2.9
20	0	0	0	0	0	0
750	750	750	1.71-1.90	1.14-1.27	0.86-0.95	19.7
700	700	700	2.44-3.06	1.63-2.04	1.22-1.53	11.43
397	324	400	1.41-1.77	0.94-1.18	0.71-0.89	11.27
189	188	190	1.11-1.16	0.74-0.77	0.55--.58	8.22
120	118	121	0.8-1.06	0.53-0.71	0.40-0.53	5.7
20	20	20	0	0	0	0
500	500	500	1.44-1.98	0.96-1.32	0.72-0.99	12.6
187	186	189	0.99-1.06	0.66-0.7	0.49-0.53	8.95
133	130	136	3.24-8-5	2.17-5.67	1.63-4.25	0.8
20	20	20	0	0	0	0
325	300	350	1.0-1.94	0.67-1.30	0.5-0.97	9
192	190	193	1.01-1.58	0.76-1.06	0.50-0.79	6.09
133	130	136	3.25-5.67	2.17-3.78	1.63-2.83	1.2
20	20	20	0	0	0	0

202 20	201 20	203 20	5.13-5.77 0	3.42-3.84 0	2.56-2.88 0	1.76 0
200 20	198 20	202 20	2.90-3.05 0	1.94-2.03 0	1.45-1.53 0	3.31 0

High exh. rate (for low error age) since cooling age (mm/yr)			High exhumation rate between analyses (mm/yr)			High error age (Ma)
20°C/km	30°C/km	40°C/km	20°C/km	30°C/km	40°C/km	
1.85	1.24	0.93	1.03	0.20	0.15	21.9
3.04	2.02	1.52	75.00	50.00	37.50	13.64
1.73	1.15	0.86	2.23	1.49	1.12	12
1.36	0.91	0.68	1.54	1.03	0.77	6.56
1.26	0.84	0.63	1.26	0.84	0.63	5.22
0	0	0	0	0	0	0
1.85	1.24	0.93	2.33	0.27	0.21	21.9
2.50	1.67	1.25	7.85	5.24	3.93	14.99
1.62	1.08	0.81	2.49	1.66	1.25	11.9
1.14	0.76	0.57	0.69	0.46	0.35	7.77
1.84	1.23	0.92	1.84	1.23	0.92	4.1
0	0	0	0	0	0	0
1.85	1.24	0.93	0.99	0.20	0.15	21.9
2.97	1.98	1.49	93.75	62.50	46.87	14.33
1.69	1.12	0.84	3.44	2.30	1.72	11.47
1.03	0.69	0.52	1.37	0.91	0.68	8.48
0.89	0.59	0.44	0.89	0.59	0.44	7.3
0	0	0	0	0	0	0
1.90	1.27	0.95	4.26	2.84	2.13	17.4
0.94	0.63	0.47	0.33	0.22	0.16	9.41
7.25	4.83	3.63	7.25	4.83	3.63	2
0	0	0	0	0	0	0
1.83	1.22	0.92	2.70	1.80	1.35	12
1.42	0.95	0.71	0.58	0.39	0.29	6.35
4.83	3.22	2.42	4.83	3.22	2.42	2.4
0	0	0	0	0	0	0

5.200	3.470	2.600	5.200	3.470	2.600	1.960
2.750	1.830	1.370	2.750	1.830	1.370	3.410

Low exh. rate (for high error age) since cooling age (mm/yr)			Low exhumation rate between analyses (mm/yr)			Center
20°C/km	30°C/km	40°C/km	20°C/km	30°C/km	40°C/km	age (Ma)
1.67	1.11	0.83	0.88	0.20	0.15	20.8
2.49	1.66	1.25	11.46	7.64	5.73	12.04
1.27	0.84	0.63	1.23	0.82	0.62	11.5
1.30	0.86	0.65	2.57	1.72	1.29	6.46
0.97	0.64	0.48	0.97	0.64	0.48	4.67
0.00	0.00	0.00	0	0	0	0
1.67	1.11	0.83	1.50	0.24	0.18	20.8
2.27	1.51	1.13	6.08	4.06	3.04	14.3
1.28	0.85	0.64	1.65	1.10	0.82	11.8
1.08	0.72	0.54	0.89	0.59	0.44	7.64
1.26	0.84	0.63	1.26	0.84	0.63	3.5
0.00	0.00	0.00	0	0	0	0
1.67	1.11	0.83	0.90	0.22	0.17	20.8
2.37	1.58	1.19	6.57	4.38	3.29	12.88
1.33	0.88	0.66	2.27	1.52	1.14	11.37
0.99	0.66	0.50	2.97	1.98	1.48	8.35
0.67	0.45	0.34	0.67	0.45	0.34	6.5
0.00	0.00	0.00	0	0	0	0
1.38	0.92	0.69	1.96	1.31	0.98	15
0.88	0.59	0.44	0.38	0.25	0.19	9.18
2.75	1.83	1.38	2.75	1.83	1.38	1.4
0.00	0.00	0.00	0	0	0	0
1.17	0.78	0.58	0.97	0.65	0.49	10.5
1.34	0.89	0.67	0.76	0.51	0.38	6.22
2.29	1.53	1.15	2.29	1.53	1.15	1.8
0.00	0.00	0.00	0	0	0	0

4.62	3.08	2.31	4.62	3.08	2.31	1.86
0.00	0.00	0.00	0	0	0	0
2.61	1.74	1.30	2.61	1.74	1.30	3.36
0.00	0.00	0.00	0	0	0	0

Exhumation rate (for center age) since cooling age (mm/yr)			Exh. rate between analyses (for center age) (mm/yr)			Between these two analyses:
20°C/km	30°C/km	40°C/km	20°C/km	30°C/km	40°C/km	
1.75	1.17	0.88	0.91	0.19	0.14	Peak to Mon
2.82	1.88	1.41	28.06	18.70	14.03	Mon-Ar
1.64	1.09	0.82	2.03	1.36	1.02	Ar-Zhe
1.33	0.89	0.67	1.96	1.30	0.98	Zhe-AFT
1.09	0.73	0.55	1.09	0.73	0.55	AFT-surface
0.00	0.00	0.00	0	0	0	
1.75	1.17	0.88	1.84	0.26	0.19	Peak to Mon
2.38	1.59	1.19	6.06	4.04	3.03	Mon-Ar
1.60	1.06	0.80	2.49	1.66	1.24	Ar-Zhe
1.11	0.74	0.56	0.79	0.52	0.39	Zhe-AFT
1.50	1.00	0.75	1.50	1.00	0.75	AFT-surface
0.00	0.00	0.00	0	0	0	
1.75	1.17	0.88	0.93	0.21	0.16	Peak to Mon
2.64	1.76	1.32	10.03	6.69	5.02	Mon-Ar
1.66	1.11	0.83	3.44	2.30	1.72	Ar-Zhe
1.01	0.67	0.51	1.86	1.24	0.93	Zhe-AFT
0.77	0.51	0.38	0.77	0.51	0.38	AFT-surface
0.00	0.00	0.00	0	0	0	
1.60	1.07	0.80	2.69	1.79	1.34	Mon-Zhe
0.91	0.61	0.45	0.35	0.23	0.17	Zhe-AFT
4.04	2.69	2.02	4.04	2.69	2.02	AFT-surface
0.00	0.00	0.00	0	0	0	
1.45	0.97	0.73	1.55	1.04	0.78	Peak to Zhe
1.38	0.92	0.69	0.67	0.44	0.33	Zhe-AFT
3.14	2.09	1.57	3.14	2.09	1.57	AFT-surface
0.00	0.00	0.00	0	0	0	

4.89	3.26	2.45	4.89	3.26	2.45	**Zhe-surface**
0.00	0.00	0.00	0	0	0	

2.68	1.79	1.34	2.68	1.79	1.34	**Zhe-surface**
0.00	0.00	0.00	0	0	0	

Exh. between these two ages	cooling rates between these two ages
20.8-12.-4	5.95
12.04-11.5	561.11
11.5-6.46	40.67
6.46-4.67	39.11
4.67-0	21.84
20.8-14.3	7.69
14.3-11.8	121.20
11.8-7.64	49.76
7.64-3.5	15.70
3.5-0	30.00
20.8-12.88	6.31
12.88-11.37	200.66
11.37-8.35	68.87
8.35-6.5	35.00
6.5-0	15.23
15-9.18	36.08
9.18-1.4	6.94
1.4-0	80.71
6.22-1.8	13.35
1.8-0	62.78

1.86-0	97.85
3.36-0	53.57